https://doi.org/10.48048/tis.2023.6974

Classification of Pneumonia, Tuberculosis, and COVID-19 on Computed Tomography Images using Deep Learning

Titipong Kaewlek*, Kanoklada Tanyong, Jintana Chakkaeo, Sumaporn Kladpree, Thunyarat Chusin, Sumalee Yabsantia and Nuntawat Udee

Department of Radiological Technology, Faculty of Allied Health Sciences, Naresuan University, Phitsanulok 65000, Thailand

(*Corresponding author's e-mail: titipongk@nu.ac.th)

Received: 10 April 2023, Revised: 3 May 2023, Accepted: 28 May 2023, Published: 28 August 2023

Abstract

The accurate diagnosis of pneumonia, tuberculosis, and COVID-19 using computed tomography (CT) images is critical for radiologists. Artificial intelligence (AI) has been introduced as a tool to aid in rapid diagnosis. In this study, we evaluated 4 deep learning models, including AlexNet, GoogleNet, ResNet, and deep convolutional neural network (DCNN), to classify CT images of tuberculosis, pneumonia, and COVID-19. We collected 2,134 normal images, 943 images of tuberculosis, 2,041 images of pneumonia, and 3,917 images of COVID-19 from online datasets. To assess the efficiency of the models, we measured their image classification performance such as accuracy, F1 score, and area under the curve. Our performance evaluation indicated that ResNet was the highest-performing model, with the best accuracy, F1 score, and area under the curve (0.966, 0.931, 0.954, respectively). The second-best performing model was DCNN, while AlexNet and GoogleNet had the next-best performance, respectively. The deep learning models exhibit a capability that could be viewed as a substitute for predicting lung diseases and could be employed to support radiologists in CT image screening.

Keywords: Deep learning, Computed tomography image, Pneumonia, Tuberculosis, COVID-19

Introduction

The modern medical imaging modality plays a crucial role in helping doctors diagnose various abnormalities in patients. One of the most commonly used imaging modalities is computed tomography (CT), which creates 3-dimensional images of organs and presents more details than traditional X-ray radiography [1,2].

The COVID-19 epidemic continues to be pervasive around the world. In April 2022, the World Health Organization (WHO) reported more than 6 million attributable deaths in addition to over 500 million confirmed cases of infection [3]. X-ray radiography and CT imaging are interesting options to diagnose COVID-19. However, lesions of COVID-19 in chest X-ray radiography and CT imaging have similar characteristics to pneumonia and tuberculosis lesions, such as ground-glass opacity, fibrosis, and consolidation [4,5], which the specialist radiologist is required to classify. As mentioned, these infections can cause similar symptoms and can be difficult to distinguish from one another based on CT images alone.

In chest CT images, one of the most difficult things to classify is distinguishing between different types of lung disease, such as those caused by tuberculosis, pneumonia, and COVID-19. CT images of patients with tuberculosis typically show diffuse or patchy areas of lung infiltration, often with a nodular or reticulonodular pattern [6]. Pneumonia caused by bacterial or viral infections can appear on CT images as patchy areas of lung infiltration, typically with a more homogeneous appearance than tuberculosis. Ground-glass opacity, which are hazy areas of lung tissue that appear darker than normal [7,8]. CT images of COVID-19 often show diffuse or patchy areas of lung infiltration, with a ground-glass opacity appearance being the most common pattern. Consolidation, which are denser areas of lung tissue that appear white on CT images [9-11].

There is significant overlap in the imaging features of these 3 diseases, and the final diagnosis is often based on a combination of clinical, laboratory, and imaging findings. Additionally, the imaging features can vary depending on the stage of the disease and the individual patient. The characteristic features of these infections on CT images are often subtle and can overlap, making it difficult for radiologists.

A previous study reported that a lack of expert radiologists may affect the screening and interpretation of lung diseases and COVID-19 [12]. Therefore, the diagnosis of lung diseases and COVID-19 is a

challenge in the field of medicine. Automatic programming called computer-aided diagnosis (CAD) is a system that can help radiologists decide and analyze abnormalities in radiographs [13].

Despite the progress made in this field, there are still concerns when it comes to classifying lung diseases from CT images, such as high variability in imaging features, overlap in imaging features, limited dataset, data bias, limited interpretability, and limited performance in low-resource settings [14,15].

Computer-aided diagnosis is an efficient and high-performance technology that uses Artificial Intelligence (AI) to detect and classify specific diseases [16]. Machine learning and deep learning are methods that enable the learning and classification of information from image data and feature extraction of images [17]. Deep learning generates high-performance models that are used to predict and classify diseases [18]. The accuracy of diagnostics is necessary. Therefore, deep learning can help correct the problems according to the similar lesions on chest radiographs.

The deep learning architecture is designed with complex layers of a neural network to increase the efficacy of learning and identify different structures in images. Radiology uses deep learning to classify breast lesions [19], brain lesions [20], lung diseases [21-23], etc. The different neural network layers of the model are referred to in the performance of deep learning.

Deep learning is a form of artificial intelligence used to learn features and then classify groups of images. Several studies have reported on the classification of multi-diseases such as cancer, pneumonia, tuberculosis, and COVID-19 in CT images using deep learning [24,25].

In recent years, deep learning has become the conventional technique for lung disease detection in CT images. Two processes, lung segmentation and lung disease classification, are recommended for detecting different diseases. In Du *et al.* [26], researchers proposed an image segmentation architecture in order to prepare the lung region image using an encoder-decoder architecture. The encoder-decoder structure is widely used in deep learning and consists of 2 components: An encoder part and a decoder part. An encoder takes variable-length sequences as input images, and a decoder acts as a conditional model, taking in the encoder input, and then leftward context the target sequence before predicting the subsequent image in the output process [27]. SegNet is one encoder-decoder model proposed by researchers [28] for semantic pixel-wise segmentation. U-Net [29] and W-Net [30] are development models of encoder-decoder architecture for image segmentation. [31] proposed U-Net for lung image segmentation on chest X-ray and reached a Dice coefficient of 0.9860, while [32,33] proposed U-Net for lung CT image segmentation with a Dice coefficient of 0.9502 and an accuracy of 0.95, respectively. Park *et al.* [34] introduced W-Net for cervix region segmentation, obtaining a result with a Dice coefficient of 0.71, while [35] proposed W-Net for Organs at Risk (OAR) segmentation on chest CT images, achieving an average dice similarity coefficient of 80.6 to 93.4 % and a Harsdorf distance of 0.5905 to 0.8961.

Regarding image classification of CT images, Alshazly *et al.* [36] studied COVID-19 and non-COVID-19 image classification using ResNet50 and obtained an accuracy of 0.81, sensitivity of 0.79, specificity of 0.90, and F1 score of 0.78. Yang *et al.* [37] adapted Fast ResNet50 and Fast ResNet152 to enable an accuracy of 0.963 and 0.962, respectively. The accuracy of ResNet152V2+GRU by Ibrahim *et al.* [38] was 0.961.

In the tuberculosis study, Lakhani and Sundaram [39] examined the use of AlexNet-TA and GoogleNet-TA for predicting tuberculosis, with an accuracy of 0.933 for AlexNet-TA and 0.953 for GoogleNet-TA. In the pneumonia study, Tan *et al.* [40] used VGG to predict pneumonia with an accuracy of 0.979. [41] used DRE-Net to extract pneumonia and normal chest CT images, achieving an accuracy of 0.94.

For multiclass image classification, Xu *et al.* [42] proposed a 3D convolutional neural network based on ResNet for classifying COVID-19, pneumonia, and normal, with an overall accuracy of 86.7 %. Nair *et al.* [43] compared 6 deep learning models, including AlexNet, VGG-16, SqueezeNet, VGG-19, ResNet-50, and CORNet to classify the COVID-19, pneumonia, and normal, CORNet is the highest performance with 94 % sensitivity, 96 % specificity, and 0.96 AUC. [44] presented CCSHNet for classifying 284 COVID-19, 281 pneumonia, 293 tuberculosis, and 306 normal CT images. The model achieved F1 scores of 96.46, 96.33, 97.64 and 97.62 % for the 4 classes, respectively.

The research process involves 3 main steps: lung segmentation, image classification, and result evaluation. The encoder-decoder model is used for lung segmentation, while the 4 models are applied to image classification. The performance of the models is evaluated using a multi-confusion matrix.

The process begins with lung segmentation, where the encoder-decoder model segments the lungs in chest CT images. The segmented images are then classified into 4 categories: Normal, pneumonia, tuberculosis, and COVID-19, using the 4 neural networks.

The objective of this study is to compare the performance of 4 models (AlexNet, GoogleNet, ResNet, and deep convolutional neural network (DCNN)) in classifying images of pneumonia, tuberculosis,

COVID-19, and normal lungs, taking into account the aforementioned difficulties and concerns associated with this task.

Materials and methods

This study consists of 2 parts: Lung segmentation and lung disease and COVID-19 classification.

Dataset preparation

This section explains the datasets used in the study. The datasets were divided into 2 parts for lung segmentation and lung disease classification.

Segmentation dataset

A total of 267 chest computed tomography (CT) images, consisting of chest CT images and mask images, were collected from Kaggle [45]. The images were in Portable Network Graphics (PNG) format with 8 bits, and the size of each image was converted to 256×256 pixels.

Lung disease classification dataset

The chest (CT) images used in this study were collected from 4 databases: Kaggle [45], Github [46], Radiopedia [47], and The National Genomics Data Center, Mendeley Data [48]. The images for classification consisted of 9,035 chest CT images, including 2,134 normal chests, 2,041 with pneumonia, 943 with tuberculosis, and 3,917 with COVID-19. The images were divided into 3 sets: 70.0 % for the training set, 20.0 % for the validation set, and 10.0 % for the test set. All images were converted to Portable Network Graphics (PNG) format with 256×256 pixels and 8 bits.

Methods

Figure1 show the diagram of this study, consists of 2 parts: Image segmentation and image classification. The model architecture of the image segmentation was an encoder-decoder model, and 4 models (AlexNet, GoogleNet, ResNet, and DCNN) were used for the classification. Both sections were processed using a graphic processing unit (GPU: Tesla P100-PCIE) of Google Colab Pro [49].

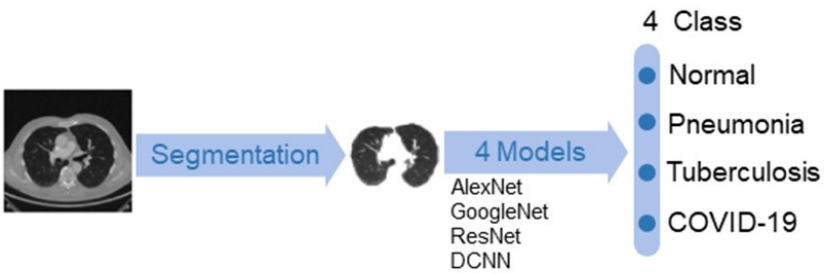

Figure 1 Diagram of this study.

Training for lung segmentation

Chest CT images were segmented using the encoder-decoder model [50]. The architecture of the model is shown in **Table 1** and **Figure 2**. The 267 chest CT images were converted to 256×256×1 pixel. The images were processed by 3 layers of convolutional (3×3) with the rectified linear activation function (Relu) followed by max pooling (2×2). Before the decoder process, the images were transferred from the encoder to the decoder by a dense (128) layer with the Relu function. The transfer image was processed by 3 upsampling (2×2) layers and followed by convolutional (3×3) with the sigmoid function. Finally, the output error was evaluated by binary cross-entropy loss and accuracy. The image segmentation model was trained using a learning rate of 0.2 with a lower bound on a learning rate of 0.00001. The network training was set to a batch size of 32 for 100 epochs. The trained model was used to segment the lung region of the initial image in the image classification section.

Table 1 Encoder - decoder model to segment the initial computed tomography image [50].

Convolutional Encoder	Convolutional Decoder
Input, 256×256×1	Output, loss + Accuracy
Conv2D (3×3, 32) + Relu MaxPooling 2×2	UpSampling 2×2 Conv2D (3×3, 1) + Sigmoid
Conv2D (3×3, 64) + Relu MaxPooling 2×2	UpSampling 2×2 Conv2D (3×3, 64) + Sigmoid
Conv2D (3×3, 128) + Relu MaxPooling 2×2	UpSampling 2×2 Conv2D (3×3, 128) + Sigmoid
Dense 128 + Relu (Encoder transfer to Decoder)	

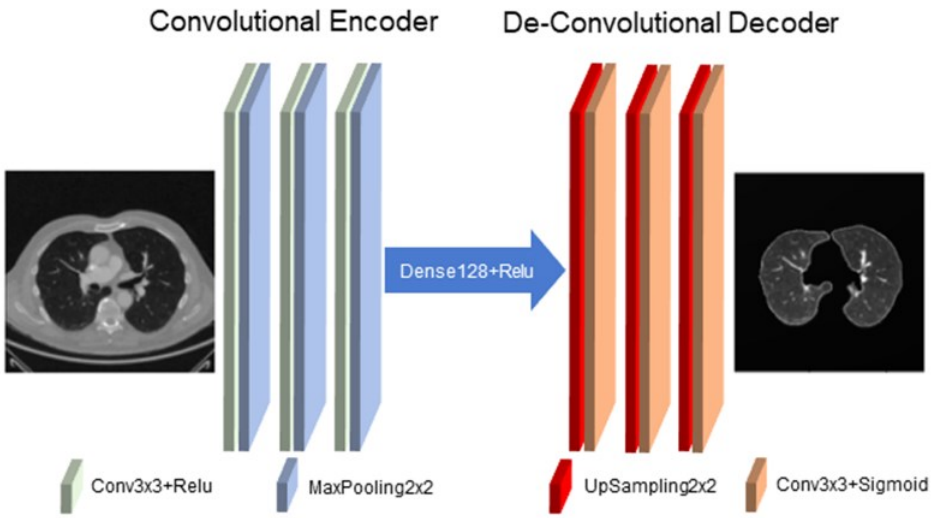

Figure 2 The encoder - decoder model.

Structure of 4 models

This study introduces 4 models, including AlexNet, GoogleNet, ResNet, and DCNN, for comparing the performance of lung CT image classification for 4 classes (tuberculosis, pneumonia, COVID-19, and normal). **Table 2** and **Figure 3** show the different structures of the 4 models. Each model consists of 5 blocks. The first input layer of the 4 models was similar at 256×256×1. The first to fifth blocks were varied by each architecture, and the output layer of the 4 models was a dense layer with Softmax (4 classes of tuberculosis, pneumonia, COVID-19, and normal).

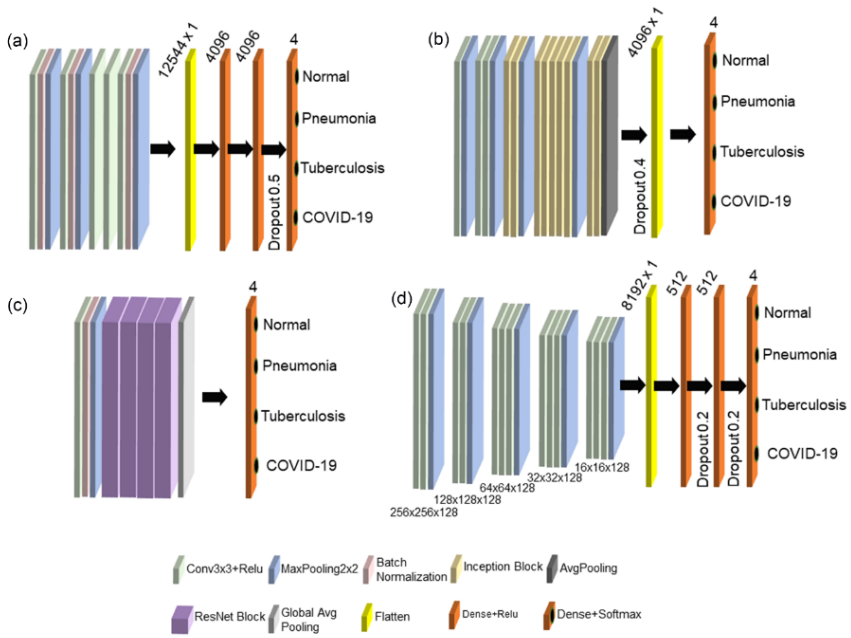

Figure 3 The structure of 4 models (a) AlexNet, (b) GoogleNet, (c) ResNet, and (d) DCNN.

Training for lung disease classification

To train the model, all 9,035 Chest CT Images in the classification dataset were segmented in the lung region using the segmentation method trained by the encoder-decoder model. Subsequently, the segmented images in the training (70 %) and validation (20 %) sets were processed by 4 models (AlexNet, GoogleNet, ResNet, and DCNN) for training and verification. The training parameters consisted of a batch size of 32 for 60 epochs. The optimizer used was the Adam method, and the loss function used was cross-entropy. The accuracy was evaluated. The test set (10 % of chest CT images) was evaluated by the 4 models, and their performance was compared. The accuracy of the training phases for AlexNet was 0.998 with a loss of 0.00058, while the accuracy of GoogleNet was 0.991 with a loss of 0.0354, the accuracy of ResNet was 0.999 with a loss of 0.0025, and the accuracy of DCNN was 1.000 with a loss of 7.8e-08.

Table 2 The structure of 4 models (AlexNet, GoogleNet, ResNet, and DCNN model).

Model	AlexNet	GoogleNet	Residual Network (ResNet)	Deep convolutional neural network (DCNN)
Input layer	256×256×1	256×256×1	256×256×1	256×256×1
1st Blocks	A Conv + Relu + a batch normalization + a MaxPooling	A Conv + Relu + a MaxPooling	A Conv + a batch normalization + Relu + a MaxPooling	Two Conv + Relu + a MaxPooling
2nd Block	A Conv + Relu + a batch normalization + a MaxPooling	Two Conv+ Relu + a MaxPooling	A ResNet block+ GlobalAvePooling	Two Conv + Relu + a MaxPooling
3rd Block	A Conv + Relu	Two inceptions + MaxPooling	A ResNet block+ GlobalAvePooling	Three Conv + Relu + a MaxPooling
4th Block	A Conv + Relu	Five inceptions + MaxPooling	A ResNet block+ GlobalAvePooling	Three Conv + Relu + a MaxPooling
5th Block	A Conv + Relu + a batch normalization + a MaxPooling	Two inceptions + AvePooling (0.4 dropout)	A ResNet block + GlobalAvePooling	Three Conv + Relu + a MaxPooling
Output layer	A flattened layer Two dense layers + Relu, the second dense layer (0.5 dropout) + Softmax (4 class)	A flattened layer Two dense layers + Softmax (4 class)	A dense + Softmax (4 class)	A flattened layer Two dense layers (0.2 dropout) + Softmax (4 class)

Conv = Convolutional, Relu = Rectified linear unit

Performance evaluation

The performance of the 4 models (AlexNet, GoogleNet, ResNet, and DCNN) was evaluated using a multi-confusion matrix that classified 4 types of chest CT images (normal, pneumonia, tuberculosis, and COVID-19). The matrix describes the performance of the classifier in 4 terms:

True Positives (TP): Model detects correctly classified normal, pneumonia, tuberculosis, and COVID-19 images.

True Negatives (TN): Model cannot detect lesions on non-lesion images.

False Positives (FP): Model detects a lesion on a non-lesion or incorrect lesion.

False Negatives (FN): Model cannot detect lesions on an image with a lesion.

The accuracy, sensitivity (recall, true positive rate (TPR)), specificity, positive predictive value (PPV, precision), negative predictive value (NPV), F1 score, false positive rate (FPR), true negative rate (TNR), false negative rate (FNR), area under curve (AUC) [51], positive likelihood ratio (LR+), and negative likelihood ratio (LR-) were calculated using Eqs. (1) - (12) to evaluate the performance of the 4 models on the multi-confusion matrix.

$$\text{Accuracy} = \frac{TP+TN}{TP+TN+FP+FN} \tag{1}$$

$$\text{Sensitivity (recall, TPR)} = \frac{TP}{TP+FN} \tag{2}$$

$$\text{Specificity} = \frac{TN}{TN+FP} \tag{3}$$

$$\text{Positive predictive value(precision)} = \frac{TP}{TP+FP} \tag{4}$$

$$\text{Negative predictive value} = \frac{TP}{TP+FP} \tag{5}$$

$$\text{F1- score} = 2\times\frac{\text{precision}\times\text{recall}}{\text{prescision}+\text{recall}} \tag{6}$$

$$\text{False positive rate (FPR)} = \frac{FP}{TN+FP} \tag{7}$$

$$\text{True negative rate (TNR)} = \frac{TN}{TN+FP} \tag{8}$$

$$\text{False negative rate (FNR)} = \frac{FN}{TP+FN} \tag{9}$$

$$\text{Area under curve(AUC)} = \frac{1}{2}\left(\frac{TP}{TP+FN}+\frac{TN}{TN+FP}\right) \tag{10}$$

$$\text{Positive likelihood ratio (LR+)} = \frac{\text{sensitivity}}{\text{1-specificity}} \tag{11}$$

$$\text{Negative likelihood ratio (LR-)} = \frac{\text{1-sensitivity}}{\text{specificity}} \tag{12}$$

Eq. (1) was used to evaluate the ability of the models to correctly label the 4-class data inputs. Eqs. (2) and (3) were used to determine the positive and negative examples of images, while Eqs. (4) and (5) were used to assess the accuracy of the model's predictions for positive and negative image examples. Eqs. (7) - (9) were used to measure the frequency of the model's predictions for positive and negative image examples. Eqs. (6), (10) - (12) were employed to evaluate the model's ability to distinguish between positive and negative image examples.

Results

In this study, 9,035 chest CT images obtained from 4 online datasets were segmented using an encoder-decoder model to isolate the lung region. **Figure 4** depicts the initial chest CT image, the ground truth masks, the masks generated by the encoder-decoder model, and the area of the generated mask on the chest CT images, demonstrating the high performance of the lung segmentation model. The segmented

shape of the lungs and the ground truth masks were closely related, with the lung segmented area completely covering the lung region.

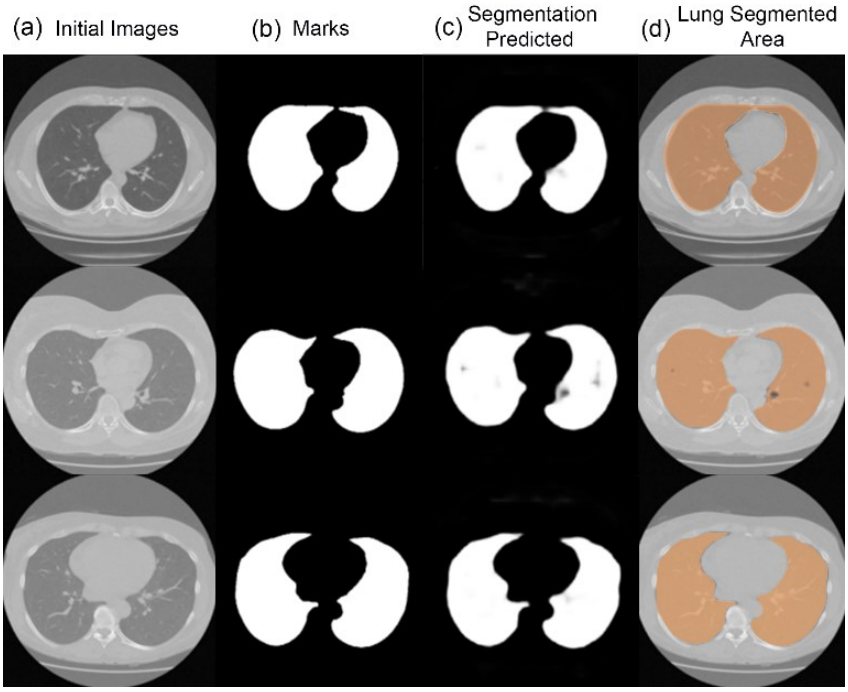

Figure 4 The result of lung segmentation images (a) Initial images, (b) Marks, (c) Segmentation predicted, and (d) lung segmentation area.

The lung segmented CT test image group was classified using 4 classification model architectures: AlexNet, GoogleNet, ResNet, and DCNN. The confusion matrix of the 4 models is shown in **Figure 5**. All 4 models demonstrated high-performance decision for image classification. The matrix is crucial, and the true positive value indicates that the 4 models can classify pneumonia, tuberculosis, COVID-19, and normal CT images.

Figure 6 shows the accuracy values closely. The accuracy of both ResNet and GoogleNet models for normal images was 0.931, DCNN was 0.917, and AlexNet was 0.915. The accuracy for pneumonia was highest in ResNet (0.997), followed by DCNN (0.980), AlexNet (0.973), and GoogleNet (0.956). The accuracy for tuberculosis was highest in AlexNet (1.000), followed closely by ResNet (0.999), DCNN (0.994), and GoogleNet (0.978). The accuracy for COVID-19 was highest in ResNet (0.936), followed by DCNN (0.912), GoogleNet (0.901), and AlexNet (0.899).

The sensitivity and negative predictive value were trending like the accuracy. The ResNet model had the highest sensitivity for normal and pneumonia, with 0.994 and 0.990, respectively. Except for tuberculosis, where AlexNet (1.000) was higher than ResNet (0.999), and in the case of COVID-19, where DCNN (0.967) was higher than ResNet (0.887). The negative predictive value of ResNet for normal and pneumonia was 0.999 and 0.997, respectively. AlexNet (1.000) had the highest negative predictive value for tuberculosis, while for COVID-19, DCNN was the highest with 0.979.

The specificity and positive predictive value of DCNN were the highest for normal and pneumonia. The specificity was 0.970, 0.967, and the positive predictive value was 0.907, 1.000, respectively. In the case of COVID-19, ResNet (1.000) was the highest, and in the case of tuberculosis, ResNet, DCNN, and AlexNet had higher specificity and positive predictive values than GoogleNet (0.996 and 0.968, respectively).

ResNet was the highest in F1 score for pneumonia and COVID-19 (0.993 and 0.931, respectively). For tuberculosis, AlexNet (1.000) remained the highest, and in the case of normal, DCNN (0.838) was the highest, followed by GoogleNet (0.836), ResNet (0.832), and AlexNet (0.815).

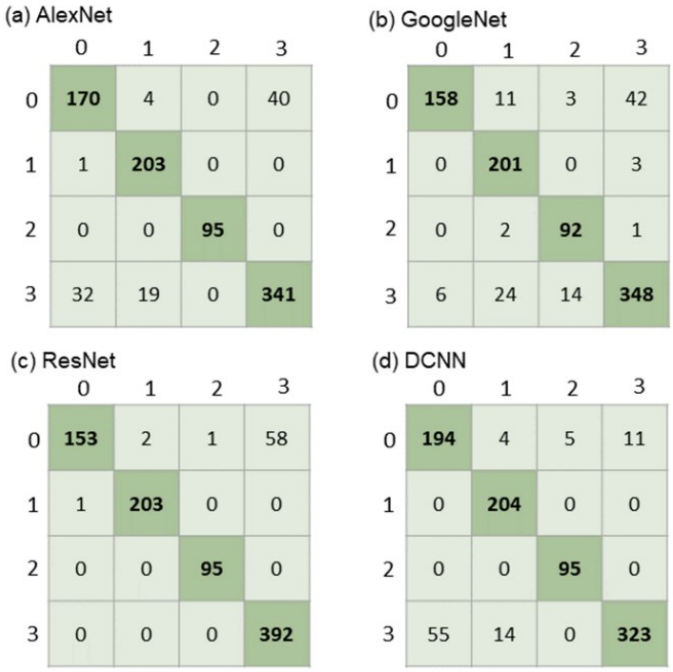

Figure 5 The confusion matrix of (a) AlexNet, (b) GoogleNet, (c) ResNet, and (d) DCNN.

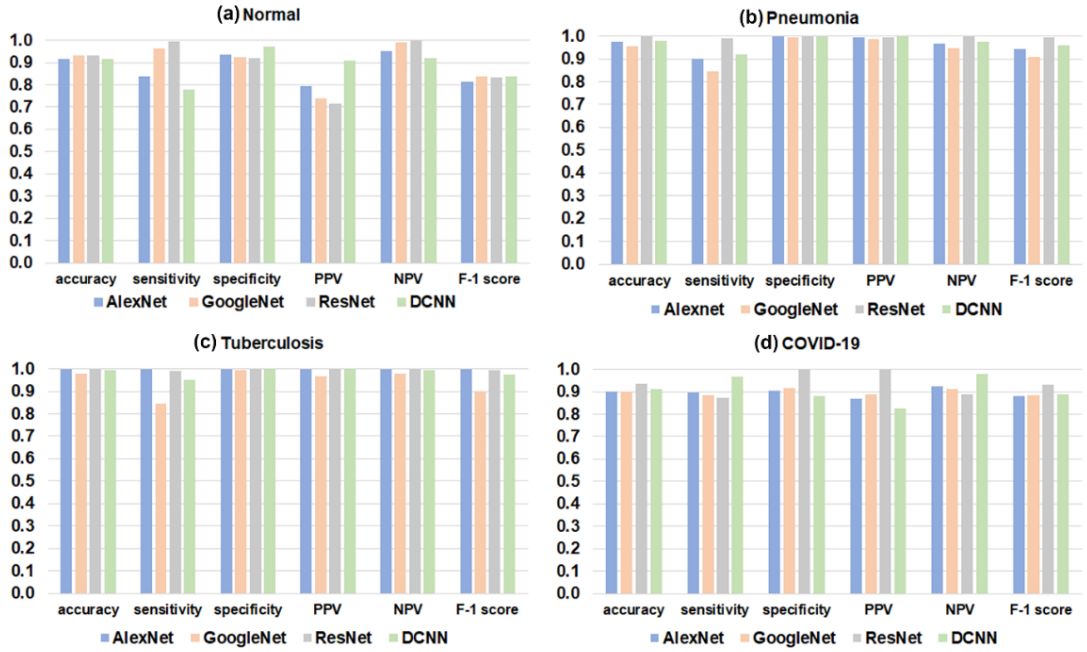

Figure 6 The performance for model correctly label data, ability of model determines, and accuracy predicts the positive and negative images of 4 model (a) AlexNet, (b) GoogleNet, (c) ResNet, and (d) DCNN.

Table 3 The result of evaluation of ability of model prediction for frequently the accuracy of the model's predictions for positive and negative image, and evaluate the model's ability to distinguish between positive and negative image of the 4 models (AlexNet, GoogleNet, ResNet, and DCNN) for each image group.

		TPR	TNR	FPR	FNR	AUC	LR+	LR-
Normal	AlexNet	0.837	0.937	0.063	0.163	0.887	13.361	0.173
	GoogleNet	0.963	0.924	0.076	0.037	0.944	12.748	0.040
	ResNet	0.994	0.919	0.081	0.006	0.956	12.232	0.007
	DCNN	0.779	0.970	0.030	0.221	0.874	25.555	0.228
Pneumonia	AlexNet	0.898	0.999	0.001	0.102	0.948	609.898	0.102
	GoogleNet	0.845	0.996	0.004	0.155	0.920	187.769	0.156
	ResNet	0.990	0.999	0.001	0.010	0.994	693.171	0.010
	DCNN	0.919	1.000	0.000	0.081	0.959	inf	0.081
Tuberculosis	AlexNet	1.000	1.000	0.000	0.000	1.000	inf	0.000
	GoogleNet	0.844	0.996	0.004	0.156	0.920	223.951	0.157
	ResNet	0.990	1.000	0.000	0.010	0.995	inf	0.010
	DCNN	0.950	1.000	0.000	0.050	0.975	inf	0.050
COVID-19	AlexNet	0.895	0.903	0.097	0.105	0.899	9.196	0.116
	GoogleNet	0.883	0.914	0.086	0.117	0.899	10.258	0.128
	ResNet	0.871	1.000	0.000	0.129	0.936	inf	0.129
	DCNN	0.967	0.879	0.121	0.033	0.923	8.003	0.037

TPR =True positive rate / TNR = True negative rate / FPR = False positive rate / FNR = False negative rate/ AUC =Area under curve / LR+ =Positive likelihood ratio / LR- =Negative likelihood ratio/ inf = infinity value

Table 3 shows the results of evaluating the models' ability to predict positive and negative images, and their ability to distinguish between the 2. The AUC indicates the model's ability to distinguish between positive and negative images, calculated using Eq. (10) which represents the AUC originated from the true positive rate and true negative rate. ResNet had the highest AUC for normal, pneumonia, and COVID-19 (0.956, 0.994, and 0.936, respectively), while AlexNet was highest for tuberculosis (1.0).

LR+ represents the probability of a positive prediction from the model, and ResNet had the highest LR+ value for pneumonia, while it was infinity for tuberculosis and COVID-19. DCNN had the highest LR+ for normal images. The infinity value occurred because of the equation of LR+ which is equal to sensitivity/(1-specificity), and the specificity value being equal to 1.0. The LR+ of DCNN for pneumonia, AlexNet, ResNet, and DCNN for tuberculosis, and ResNet for COVID-19 were infinity (inf) values.

LR- represents the probability of a negative prediction from the model, and ResNet had the highest LR- value for normal and pneumonia. AlexNet remained the best model for tuberculosis, and DCNN was the best model for COVID-19.

Table 4 The result of overall performance of the model's ability to distinguish between positive and negative image of the 4 models (AlexNet, GoogleNet, ResNet, and DCNN).

	accuracy	sensitivity	specificity	F1 score	AUC	LR+	LR-
AlexNet	0.947	0.894	0.965	0.894	0.929	25.281	0.110
GoogleNet	0.941	0.883	0.961	0.883	0.922	22.613	0.122
ResNet	0.966	0.931	0.977	0.931	0.954	40.790	0.070
DCNN	0.951	0.902	0.967	0.902	0.934	27.506	0.102

AUC =Area under curve / LR+ =Positive likelihood ratio / LR- =Negative likelihood ratio

Table 4 confirm that the ResNet is the best model for classification the 4 lung lesions (pneumonia, tuberculosis, COVID-19, and normal) of CT images. Secord is DCNN, third is AlexNet, and then GoogleNet, respectively.

Discussion

In this study, we compared 4 models (AlexNet, GoogleNet, ResNet, and DCNN) for classifying 4 types of lung lesions (pneumonia, tuberculosis, COVID-19, and normal) in CT images. The input image was a 256×256×1 matrix size lung segmentation, saved as an 8-bit PNG file format. We used 4 different input image datasets without any preprocessing for training, validation, and testing. During training, the AlexNet, GoogleNet, ResNet, and DCNN models were trained using a batch size of 32 for 60 epochs, with the Adam optimizer, binary cross-entropy loss, and accuracy metric. Results were compared using multiple confusion metrics, and the ResNet model performed the best in terms of accuracy of model prediction, correctly predicting the labels for all 4 classes of input data (tuberculosis, pneumonia, COVID-19, and normal).

The F1 score indicates the recall or sensitivity and precision of the model. Recall and precision are common metrics that take into account class imbalance. The F1 score is an average of both values and weights the recall and precision, showing the model's overall performance. In this work, we found that the ResNet model had the highest F1 score.

Moreover, the AUC, LR+, and LR- can describe the ability of the model to distinguish between positive and negative images. The AUC in this study was calculated using the influence of true positive rate and true negative rate, indicating the model's ability for positive and negative results of model prediction [51]. To test the clinical viewpoint of the model, we calculated the likelihood ratio for positive and negative test results to confirm the F1 score and AUC. The positive likelihood ratio (LR+) tests the probability of a positive image, given the image has no positive result. Conversely, the negative likelihood ratio (LR-) tests the probability of a negative image, given the image has no negative result [52,53]. Results show that the AUC, LR+, and LR- of the ResNet model were the best for distinguishing between positive and negative images.

Table 5 shows a comparison between previous studies and our own. Chuansheng Zheng et al. [54] used a dataset from Union Hospital, Tongji Medical College, Huazhong University of Science and Technology, China, which consisted of 540 patients, including 313 COVID-19 and 229 other images. The U-Net architecture was used for lung segmentation, and DeCovNet classified the image class. DeCovNet was divided into 3 stages: The first was a convolution layer, the second had 2 ResNet blocks, and the third was a progressive classification layer with softmax. The accuracy was 90.1 %, AUC was 0.95, sensitivity was 90.7 %, and specificity was 90.11 %. However, the imperfect ground-truth mask affected the lung segmentation, and a dataset and cross-center validation were not performed.

Li *et al.* [55] collected 4,536 chest CT images from 3,506 patients at 6 medical centers, including 1,296 COVID-19, 1,735 pneumonia, and 1,325 normal images. The U-Net architecture was used for lung segmentation, and the CovNet consisted of a ResNet50 backbone for image classification. The AUC was 0.96 %, sensitivity was 90.0 %, and specificity was 96.0 %.

S Walvekar and S Shinde [56] collected 359 images of COVID-19, pneumonia, and normal images from Joseph Paul Cohen, Paul Morrison, and Lan Dao's collection. The images were augmented by vertical flip only to increase the dataset size. There was no lung segmentation step, and the augmented images were classified by ResNet50 with an input image size of 224×224×3. The accuracy was 96.23 %, F1 score was 0.963, sensitivity was 97.15 %, and precision was 95.60 %.

Lahsaini *et al.* [57] collected 4,986 CT images of 177 patients, including 1,868 COVID-19 and 3,118 other diseases, from the University Hospital of Tlemcen, Algeria. The images were augmented by rotation, width shift, height, rescale, shear range, zoom range, horizontal flip, and vertical flip. The input image size was 128×128×3, and the Densenet201 base was used for classification. The accuracy was 98.8 %, AUC was 0.98, sensitivity was 98.54 %, and specificity was 99.22 %.

Zhang *et al.* [58] collected 29,278 images (9,420 COVID-19, 9,858 pneumonia, and 10,000 normal) with a 32×32 image size from 2019nCoVR. SegNet-Lung model with a U-net architecture was use for lung segmentation. The CapsNet was used for classification, and the accuracy was 84.29 %.

The objective of image segmentation is to select the structures in medical images. Due to the high efficiency and accuracy of model learning, segmentation of the initial image can help improve classification [59]. Previous studies indicate that segmentation techniques for lung segmentation improve the performance of image classification [60]. The U-Net architecture is a commonly used technique for segmentation in medical images [61,62]. Other techniques include convolutional neural networks (CNNs), recurrent neural networks (RNNs) and long short-term memory (LSTM), encoder-decoders, and generative adversarial networks (GANs) [63]. The evaluation of segmentation performance can be analyzed by dice score, volume overlap error, and relative volume difference for region quality analysis; average symmetric surface distance, and maximum symmetric surface distance for surface distance quality analysis [59]. High-

quality segmentation improves the learning of the model. In this work, we use an encoder-decoder model with a similar architecture to U-Net, but without the contracted path that concatenates the layers of downsampling and upsampling steps. The results of our work show that the predicted lung area completely superimposes on the ground truth marks.

The input image size of this study was 256×256×1, which is larger than other works. For instance, [57] used a 128×128×3 matrix size, while [54] used a 32×32 matrix size. The image size influences the learning of the model, with larger sizes being more prone to overfitting than smaller sizes [64]. However, high image resolution can improve the performance of image classification [65,66]. In addition to the complexity of the model, dropout techniques, image augmentation, and the number of epochs can also affect overfitting [67].

Table 5 The comparative analysis of previous publications.

Author	Dataset	Lung segmentation methods	Classification Images methods	Result
Zheng *et al.* [54]	313 COVID-19, 229 others images	U-Net	DeCovNet	Accuracy: 90.1 % AUC: 0.95
Li *et al.* [55]	1296 COVID-19, 1735 pneumonia, 1325 normal	U-net	CoVNet	Sensitivity: 90.0 % Specificity: 96.0 % AUC: 0.96
Walvekar and Shinde [56]	359 images (COVID-19, pneumonia, normal)	-	ResNet50	Accuracy: 96.23 % F1 score: 0.96
Lahsaini *et al.* [57]	1,868 COVID-19, 3,118 normal and other	-	DenseNet201	Accuracy: 98.8 % AUC: 0.98
Zhang *et al.* [58]	9,858 pnuemonia, 9,420 COVID-19, 10,000 normal	SegNet-Lung	CapsNet	Accuracy: 84.29 %
This study	2,041 pneumonia, 943 tuberculosis, 3,917 COVID-19, 2,134 normal	Encoder - decoder model	ResNet	Accuracy: 96.66 % AUC: 0.95 %

The limitations of this study can be attributed to 2 reasons that may improve the performance of classification. Firstly, the number of images used for this study. A total of 9,035 Chest CT Images (2,041 pneumonia, 943 tuberculosis, 3,917 COVID-19, and 2,134 normal) were used, which is a small dataset that may have contributed to the decline in the performance of image classification. Image augmentation [68] is a procedure that can increase the number of images, and there are several methods, such as rotation, flipping the image angle, translation, shifting to move the image, zooming, etc. Augmentation can increase the image dataset and possibly improve the performance. However, image augmentation may reduce the performance of classification in the case of the specific shape of the organ, such as the chest X-ray [69]. Therefore, it is important to choose suitable methods of augmentation. To improve the performance of the model, increasing the number of images to create a large dataset is indeed a requirement. Kieu *et al.* [70] published a survey of image datasets for lung disease detection on chest X-ray and CT images, such as ImageCLEF2018, ImageCLEF2019 for tuberculosis, and COVID-CT dataset for COVID-19.

Secondly, the use of several dataset sources. In this study, images were collected from 4 datasets (Kaggle, Github, Radiopedia, and the National Genomics Data Center, Mendeley Data). The different file types and image sizes of the 4 image datasets were converted to PNG filename and 256×256 matrix size. The difference in image quality of the initial image may affect the process of image classification. In this study, image quality was not adjusted before training of image classification. In the case of using multiple datasets, it is necessary to adjust the details of the image in the pre-processing procedure to avoid errors in the different image information [71,72], such as image contrast enhancement [73], and image noise reduction [71]. The adaptive histogram equalization method [73] is generally used to improve the contrast of images [74]. High-contrast images are significantly easier to detect the details of different tissues on lung CT images. Additional techniques, such as contrast-limited adaptive histogram [74], bilateral histogram equalization, and recursive mean separate histogram equalization [75], may also be used.

Conclusions

In conclusion, this research introduces 4 models (AlexNet, GoogleNet, ResNet, and DCNN) and compares their performance in terms of their ability to distinguish between positive and negative images of 4 chest CT images (tuberculosis, pneumonia, COVID-19, and normal). According to the carried-out exams, the ResNet model shows the highest performance for classifying the 4 classes (tuberculosis, pneumonia, COVID-19, and normal) on chest CT images. The deep learning models demonstrate an ability that can be considered an alternative for predicting lung diseases and can be used to assist radiologists in screening CT images. In future work, we will develop a convolutional neural network to classify lung lesions such as ground-glass opacity, fibrosis, and consolidation to improve the performance of predicting lung diseases. Additionally, the techniques of image augmentation and pre-processing will vary to find the suitable procedure for lung CT image classification.

Acknowledgements

This study was supported by Naresuan University (NU), and National Science, Research and Innovation Fundamental Fund (NSRF). Grant NO. (R2565B090). This study approved by the ethics committee of Naresuan University, Thailand (IRB No. P10111/64).

References

[1] E Bercovich and CM Javitt. Medical imaging: From roentgen to the digital revolution, and beyond. *Rambam Maimonides Med. J.* 2018; **9**, e0034.
[2] J Hsieh and T Flohr. Computed tomography recent history and future perspectives. *J. Med. Imag.* 2021; **8**, 052109.
[3] World Health Organization. Weekly epidemiological update on COVID-19 - 20 April 2022, Available at: https://www.who.int/publications/m/item/weekly-epidemiological-update-on-COVID-19--20-april-2022, accessed April 2022.
[4] S Machnicki, D Patel, A Singh, A Talwar, B Mina, M Oks, P Makkar, D Naidich, A Mehta, NS Hill, KK Brown and S Raoof. The usefulness of chest CT imaging in patients with suspected or diagnosed COVID -19 a review of literature. *Chest* 2021; **160**, 652-70.
[5] S Du, S Gao, G Huang, S Li, W Chong, Z Jia, G Hou, YXJ Wáng and L Zhang. Chest lesion CT radiological features and quantitative analysis in RT-PCR turned negative and clinical symptoms resolved COVID-19 patients. *Quant. Imag. Med. Surg.* 2020; **10**, 1307-17.
[6] AS Bhalla, A Goyal, R Guleria and AK Gupta. Chest tuberculosis: Radiological review and imaging recommendations. *Indian J. Radiol. Imag.* 2015; **25**, 213-25.
[7] C Beigelman-Aubry and S Schmidt. *Pulmonary infections: Imaging with CT*. *In*: U Schoepf and F Meinel (Eds.). Multidetector-row CT of the thorax. Springer, Cham, Switzerland, 2016.
[8] R Eibel and J Mueller. Pulmonary infections: Pneumonia. *MRI Lung* 2017; **8**, 383-400.
[9] M Carotti, F Salaffi, P Sarzi-Puttini, A Agostini, A Borgheresi, D Minorati, M Galli, D Marotto and A Giovagnoni. Chest CT features of coronavirus disease 2019 (COVID-19) pneumonia: Key points for radiologists. *Radiol. Med.* 2020; **125**, 636-46.
[10] MM Hefeda. CT chest findings in patients infected with COVID-19: Review of literature. *Egypt. J. Radiol. Nucl. Med.* 2020; **51**, 239.
[11] X Wang, C Liu, L Hong, C Yuan, J Ding, Q Jia, G Sun, W Peng and Q Sun. CT findings of patients infected with SARS-CoV-2. *BMC Med. Imag.* 2020; **20**, 70.
[12] AH Hoog, HK Meme, HV Deutekom, AM Mithika, C Olunga, F Onyino and MW Borgdorff. High sensitivity of chest radiograph reading by clinical officers in a tuberculosis prevalence survey. *Int. J. Tuberc. Lung Dis.* 2011; **15**, 1308-14.
[13] J Melendez, CI Sánchez, RH Philipsen, P Maduskar, R Dawson, G Theron, K Dheda and BV Ginneken. An automated tuberculosis screening strategy combining X-ray-based computer-aided detection and clinical information. *Sci. Rep.* 2016; **29**, 25265.
[14] N Sourlos, J Wang, Y Nagaraj, PV Ooijen and R Vliegenthart. Possible bias in supervised deep learning algorithms for CT lung nodule detection and classification. *Cancers* 2022; **14**, 3867.
[15] L Alzubaidi, J Zhang, AJ Humaidi, A Al-Dujaili, Y Duan, OJ Santamaría, MA Fadhel, M Al-Amidie and L Farhan. Review of deep learning: Concepts, CNN architectures, challenges, applications, future directions. *J. Big Data* 2021; **8**, 53.
[16] S Wang, G Cao, Y Wang, S Liao, Q Wang, J Shi, C Li and D Shen. Review and prospective: artificial intelligence in advanced medical imaging. *Front. Radiol.* 2021; **1**, 781862.

[17] R Ahmad. The role of digital technology and artificial intelligence in diagnosing medical images: A systematic review. *Open J. Radiol*. 2021; **11**, 19-34.
[18] T Wang, Y Lei, Y Fu, FJ Wynne, JW Curran, T Liu and X Yang. A review on medical imaging synthesis using deep learning and its clinical applications. *J Appl. Clin. Med. Phys*. 2020; **22**, 11-36.
[19] T Mahmood, J Li, Y Pei, F Akhtar, MU Rehman and SH Wasti. Breast lesions classifications of mammographic images using a deep convolutional neural network-based approach. *PLoS One* 2022; **17**, e0263126.
[20] D Castillo, V Lakshminarayanan and JM Rodríguez- Álvarez. MR images, brain lesions, and deep learning. *Appl. Sci.* 2021, **11**, 1675.
[21] R Li, C Xiao, Y Huang, H Hassan and B Huang. Deep learning applications in computed tomography images for pulmonary nodule detection and diagnosis: A review. *Diagnostics* 2022; **12**, 298.
[22] AM Heuvelmans, MAP van Ooijen, S Ather, FC Silva, D Han, CP Heussel, W Hickes, HU Kauczor, P Novotny, H Peschl, M Rook, R Rubtsov, OV Stackelberg, MT Tsakok, C Arteta, J Declerck, T Kadir, L Pickup, F Gleeson and M Oudkerk. Lung cancer prediction by deep learning to identify benign lung nodules. *Lung Cancer* 2021; **154**, 1-4.
[23] M Aminu, AN Ahmad and MHM Noor. Covid-19 detection via deep neural network and occlusion sensitivity maps. *Alex. Eng. J.* 2021; **60**, 4829-55.
[24] MD Ibrahim, MN Elshennawy and MA Sarhan. Deep-chest: Multi-classification deep learning model for diagnosing COVID-19, pneumonia, and lung cancer chest diseases. *Comput. Biol. Med.* 2021; **132**, 104348.
[25] TKS Kieu, A Bade, MHA Hijazi and H Kolivand. A survey of deep learning for lung disease detection on medical images: State-of-the-Art, taxonomy, issues and future directions. *J. Imag.* 2020; **6**, 131.
[26] G Du, X Cao, J Liang, X Chen and Y Zhan. Medical image segmentation based on U-Net: A review. *J. Imag. Sci. Tech.* 2020; **64**, art00009.
[27] Dive into deep learning, Available at: https://d2l.ai/chapter_recurrent-modern/encoder-decoder.html, accessed January 2022.
[28] V Badrinarayanan, A Kendall and R Cipolla. SegNet: A deep convolutional encoder- decoder architecture for image segmentation. *IEEE Trans. Pattern Anal. Mach. Intell*. 2017; **39**, 2481-95.
[29] O Ronneberger, P Fischer and T Brox. *U- Net convolutional networks for biomedical image segmentation*. *In*: N Navab, J Hornegger, W Wells and A Frangi (Eds.). Medical image computing and computer-assisted intervention - MICCAI 2015. Springer, Cham, Switzerland.
[30] X Xia and B Kulis. W-Net: A deep model for fully unsupervised image segmentation, Available https://doi.org/10.48550/arXiv.1711.08506, accessed January 2022.
[31] E Mique Jr and A Malicdem. Deep residual U-Net based lung image segmentation for lung disease detection. *IOP Conf. Ser. Mater. Sci. Eng.* 2020; **803**, 012004.
[32] BA Skourt, AE Hassani and A Majda. Lung CT image segmentation using deep neural networks, *Procedia Comput. Sci.* 2018; **127**, 109-13.
[33] A Saood and I Hatem. COVID-19 lung CT image segmentation using deep learning methods: U-Net versus SegNet. *BMC Med. Imaging.* 2021; **21**,19.
[34] J Park, H Yang, HJ Roh, W Jung and GJ Jang. Encoder- weighted W- Net for unsupervised segmentation of cervix region in colposcopy images. *Cancers* 2022; **14**, 3400.
[35] W Zhao, H Chen and Y Lu. W-net: A network structure for automatic segmentation of organs at risk in thorax computed tomography. *In*: Proceedings of the 2020 2nd International Conference on Intelligent Medicine and Image Processing, Tianjin, China. 2020, p. 66-9.
[36] H Alshazly, C Linse, M Abdalla, E Barth and T Martinetz. Covid-nets. Deep CNN architectures for detecting COVID-19 using chest CT scans. *PeerJ Comput. Sci.* 2021; **7**, e655.
[37] D Yang, C Martinez, L Visuña, H Khandhar, C Bhatt and J Carretero. Detection and analysis of COVID-19 in medical images using deep learning techniques. *Sci. Rep.* 2021; **11**, 19638.
[38] MD Ibrahim, MN Elshennawy and MA Sarhan. Deep-chest: Multi-classification deep learning model for diagnosing COVID-19, pneumonia, and lung cancer chest diseases. *Comput. Biol. Med*. 2021; **132**, 104348.
[39] P Lakhani and B Sundaram. Deep learning at chest radiography: Automated classification of pulmonary tuberculosis by using convolutional neural networks. *Radiology* 2017; **284**, 574-82.
[40] W Tan, P Liu, X Li, Y Liu, Q Zhou, C Chen, Z Gong, X Yin and Y Zhang. Classification of COVID-19 pneumonia from chest CT images based on reconstructed super-resolution images and VGG neural network. *Health Inf. Sci. Syst.* 2021; **9**, 10.

[41] Y Song, S Zheng, L Li, X Zhang, XD Zhang, Z Huang, J Chen, R Wang, H Zhao, Y Chong, J Shen, Y Zha, Y Yang. Deep learning enables accurate diagnosis of novel coronavirus (COVID-19) with CT images. *IEEE ACM Trans. Comput. Biol. Bioinformatics* 2021; **18**, 2775-80.
[42] X Xu, X Jiang, C Ma, P Du, X Li, S Lv, L Yu, Y Chen, J Su, G Lang, Y Li, Hong Zhao, K Xu, L Ruan and W Wu. Deep learning system to screen coronavirus disease 2019 Pneumonia, Available at: https://doi.org/10.48550/arXiv.2002.09334, accessed January 2022.
[43] R Nair, A Alhudhaf, D Koundal, R I Doewes and P Sharma. Deep learning-based COVID-19 detection system using pulmonary CT scans. *Turk. J. Elec. Eng. Comput. Sci.* 2021; **29**, 2716-27.
[44] SH Wang, DR Nayak, DS Guttery, X Zhang and YD Zhang. COVID-19 classification by CCSHNet with deep fusion using transfer learning and discriminant correlation analysis. *Inform. Fusion* 2021; **68**, 131-48.
[45] Kaggle dataset, Available at: https://www.kaggle.com/datasets, accessed January 2022.
[46] Github, Available at: https://www.github.com, accessed January 2022.
[47] Radiopaedia, Available at: https://radiopaedia.org, accessed January 2022.
[48] Mendeley dataset, Available at: https://data.mendeley.com/, accessed January 2022.
[49] Colaboratory, Available at: https://colab.research.google.com/, accessed February 2022.
[50] CT Lung Segmentation, Available at: https://github.com/kairess/CT_lung_segmentation, accessed January 2022.
[51] F Idrees, M Rajarajan, M Conti, TM Chen and Y Rahulamathavan. PIndroid: A novel Android malware detection system using ensemble learning methods. *Comput. Secur*. 2017; **68**, 36-46.
[52] P Ranganathan and R Aggarwal. Understanding the properties of diagnostic tests - Part 2: Likelihood ratios. *Perspect. Clin. Res.* 2018; **9**, 99-102.
[53] CM Florkowski. Sensitivity, specificity, receiver- operating characteristic (ROC) curves and likelihood ratios: Communicating the performance of diagnostic tests. *Clin. Biochem. Rev.* 2008; **29**, S83-S87.
[54] C Zheng, X Deng, Q Fu, Q Zhou, J Feng, H Ma, W Liu and C Zheng. A weakly-supervised framework for COVID-19 classification and lesion localization from Chest CT. *IEEE Trans. Med. Imag.* 2020; **39**, 2615-25.
[55] L Li, L Qin, Z Xu, Y Yin, X Wang, B Kong, J Bai, Y Lu, Z Fang, Q Song, K Cao, D Liu, G Wang, Q Xu, X Fang, S Zhang, J Xia and J Xia. Using artificial intelligence to detect COVID- 19 and community- acquired pneumonia based on pulmonary CT: Evaluation of the diagnostic accuracy. *Radiology* 2020; **296**, E65-E71.
[56] S Walvekar and S Shinde. Detection of COVID-19 from CT images using resnet50. *In*: Proceedings of the 2nd International Conference on Communication & Information Processing, Kuala Lumpur Malaysia. 2020, p. 1-8.
[57] I Lahsaini, MEH Daho and MA Chikh. Deep transfer learning-based classification model for covid-19 using chest CT-scans. *Pattern Recognit. Lett.* 2021; **152**, 122-8.
[58] XQ Zhang, GY Wang and SG Zhao. CapsNet-COVID19: Lung CT image classification method based on CapsNet model. *Math. Biosci. Eng.* 2022; **19**, 5055-74.
[59] R Wang, T Lei, R Cui, B Zhang and H Meng. Medical image segmentation using deep learning: A survey. *IET Image Process.* 2022; **16**, 1243-67.
[60] J Moorthy and UD Gandhi. A Survey on medical image segmentation based on deep learning techniques. *Big Data Cogn. Comput.* 2022; **6**, 117.
[61] XX Yin, L Sun, Y Fu, R Lu and Y Zhang. U-Net-based medical image segmentation. *J. Healthc Eng.* 2022; **2022**, 4189781.
[62] N Siddique, S Paheding, CP Elkin and V Devabhaktuni. U-Net and its variants for medical image segmentation: A review of theory and applications. *IEEE Access.* 2021; **9**, 82031-57.
[63] S Minaee, Y Boykov, F Porikli, A Plaza, N Kehtarnavaz and D Terzopoulos. Image segmentation using deep learning: A survey, Available at: https://doi.org/10.48550/arXiv.2001.05566, accessed January 2022.
[64] O Rukundo. Effects of image size on deep learning. *Electronics* 2023; **12**, 985.
[65] CF Sabottke and BM spieler. The effect of image resolution on deep learning in radiology. *Radiol. Artif. Intell.* 2020; **2**, e190015.
[66] V Thambawita, I Strümke, SA Hicks, P Halvorsen, S Parasa and MA Riegler. Impact of image resolution on deep learning performance in endoscopy image classification: An experimental study using a large dataset of endoscopic images. *Diagnostics* 2021; **11**, 2183.
[67] X Ying. An overview of overfitting and its solutions. *J. Phys. Conf. Ser.* 2019; **1168**, 022022.

[68] C Shorten and TM Khoshgoftaar. A survey on image data augmentation for deep learning. *J. Big Data* 2019; **6**, 60.
[69] K Purohit, A Kesarwani, DR Kisku and M Dalui. COVID-19 detection on chest X-ray and CT scan images using multi-image augmented deep learning model. *bioRxiv* 2020, https://doi.org/10.1101/2020.07.15.205567
[70] STH Kieu, A Bade, MHA Hijazi and H Kolivand. A survey of deep learning for lung disease detection on medical images: state-of-the-art, taxonomy, issues and future directions. *J. Imag.* 2020; **6**, 131.
[71] S Masoudi, SA Harmon, S Mehralivand, SM Walker, H Raviprakash, U Bagci, PL Choyke and B Turkbey. Quick guide on radiology image pre-processing for deep learning applications in prostate cancer research. *J. Med. Imag.* 2021; **8**, 010901.
[72] G Philip and S George. A review of preprocessing methods and pre-trained models for COVID-19 detection using medical images. *Int. J. Eng. Res. Tech*. 2022; **10**, 236-9.
[73] A Giełczyk, A Marciniak, M Tarczewska and Z Lutowski. Pre-processing methods in chest X-ray image classification. *PLoS ONE* 2022; **17**, e0265949.
[74] FA Dawood and ZM Abood. The importance of contrast enhancement in medical images analysis and diagnosis. *Int. J. Eng. Res. Tech*. 2018; **7**, 21-4.
[75] MW Mirza, A Siddiq and IR Khan. A comparative study of medical image enhancement algorithms and quality assessment metrics on COVID-19 CT images. *Signal Image Video Process.* 2023; **17**, 915-24.